TISSUE ENGINEERING: Part A
Volume 18, Numbers 21 and 22, 2012

DOI: 10.1089/ten.tea.2011.0747

Regenerating Nucleus Pulposus of the Intervertebral Disc Using Biodegradable Nanofibrous Polymer Scaffolds

Ganjun Feng, M.D.,[1,2] Zhanpeng Zhang, M.S.,[3] Xiaobing Jin, M.D., Ph.D.,[2] Jiang Hu, Ph.D.,[2] Melanie J. Gupte, M.S.,[3] Jeremy M. Holzwarth, M.S.,[3] and Peter X. Ma, Ph.D.[2–5]

Low back pain is a leading health problem in the United States, which is most often resulted from nucleus pulposus (NP) degeneration. To date, the replacement of degenerated NP relies entirely on mechanical devices. However, a biological NP replacement implant is more desirable. Here, we report the regeneration of NP tissue using a biodegradable nanofibrous (NF) scaffold. Rabbit NP cells were seeded on the NF scaffolds to regenerate NP-like tissue both *in vitro* and in a subcutaneous implantation model. The NP cells on the NF scaffolds proliferated faster than those on control solid-walled (SW) scaffolds *in vitro*. Significantly more extracellular matrix (ECM) production (glycosaminoglycan and type II collagen) was found on the NF scaffolds than on the control SW scaffolds. The constructs were then implanted in the caudal spine of athymic rats for up to 12 weeks. The tissue-engineered NP could survive, produce functional ECM, remain in place, and maintain the disc height, which is similar to the native NP tissue.

Introduction

As many as 80% of adults experience low back pain at some point in their lives[1] with 5% developing chronic diseases.[2] The leading etiological contributor to low back pain is intervertebral disc degeneration,[1] which most often starts in the nucleus pulposus (NP).[3,4] The current clinical treatments for disc degeneration are mainly focused on the alleviation of symptoms, while the underlying biological problems remain largely unaddressed. Spine fusion is the standard surgical treatment for axial low back pain.[5,6] This treatment is intended to stop pain by eliminating motion across the joint space. However, fusion may accelerate degenerative changes in the adjacent discs.[7,8] Total disc replacement implants were developed to avoid the loss of motion at the operated level and reduce the degenerative incidences at the adjacent segments.[9] However, the procedure requires the dissection of the annulus fibrosus and endplates, which are still competent in the early stage of disc degeneration. Its long-term efficacy is a matter of much debate.[10] Prosthetic disc nucleus implants provide a less invasive treatment and preserve spinal motion segments.[11,12] However, nonbiological NP implants do not contain viable cells and do not remodel. Additionally, traditional permanent implants suffer from common complications such as polyethylene wear debris, osteolysis, and implant loosening. A tissue-engineered NP would therefore be a better alternative to the existing implants.

The tissue engineering strategy has been used to regenerate biological NP tissue in research. Various hydrogels have been used to support NP cell culture,[13–22] but the poor mechanical properties of hydrogels limit their application.[23]

The physiological properties of the intervertebral disc are linked to the structure of its extracellular matrix (ECM). The ECM in the healthy disc is a web of natural nanoscale fibers. As an artificial ECM, a scaffolding material often benefits from mimicking advantageous features of the natural ECM.[24] Previously, electrospun nanofibers were used for NP cell culture to retain the phenotype.[25] However, without designed large pores for cell penetration, the size of regenerated tissue was limited. We developed a new phase-separation technique to fabricate 3D scaffolds with highly interconnected macropores and nanofibrous (NF) matrix.[26] We hypothesized that the ECM-mimicking NF architecture could mimic the microenvironment in the healthy intervertebral disc, improving cell viability, promoting NP cell proliferation, and tissue regeneration. To test this hypothesis, the NF scaffolds were compared with control solid-walled (SW) scaffolds (made from the same material and had the same macropore structure, but without the NF feature) using three

[1]Department of Orthopaedic Surgery, West China Hospital, Sichuan University, Chengdu, Sichuan, China.
Departments of [2]Biologic and Materials Sciences and [3]Biomedical Engineering, University of Michigan, Ann Arbor, Michigan.
[4]Macromolecular Science and Engineering Center, University of Michigan, Ann Arbor, Michigan.
[5]Department of Materials Science and Engineering, University of Michigan, Ann Arbor, Michigan.

experimental models: (1) *in vitro* NP tissue engineering; (2) subcutaneous implantation for ectopic NP tissue formation; and (3) athymic rat caudal disc repair.

Materials and Methods

Preparation of NF and SW PLLA scaffolds

The NF and SW PLLA scaffolds were prepared as previously described.[26] Briefly, sugar spheres with a desired diameter range were assembled into a template. A polymer solution was then cast into the template and underwent either a phase-separation process to form the NF scaffold or a solvent-evaporation process to form the SW scaffold. The sugar sphere-assembly was then leached away in water to form the interconnected spherical pore network. The scaffolds used in the current study had a disc-like shape with a height of 1.0 mm, a diameter of either 3.2 or 2.5 mm, and a pore size of 250–420 μm. This pore size was previously found to support uniform cell seeding and distribution.[27] The average diameter of the nanofibers was between 100 and 200 nm.

Cell culture and seeding

The NF and SW scaffolds (3.2 mm in diameter) were soaked in 70% ethanol to prewet for 30 min and then the ethanol was exchanged with phosphate-buffered saline (PBS) for three times (30 min each). The scaffolds were then washed twice with Dulbecco's Modified Eagle Medium containing 10% fetal bovine serum (1 h each). NP cells were isolated from 8-week-old male New Zealand white rabbits and cultured for 2 passages following published methods.[28] Fifteen microliters NP cell suspension (3×10^7 cells/mL) was seeded on each scaffold and the cell–scaffold constructs were cultured on an orbital shaker in an incubator at 37°C with 5% CO_2. The medium was changed every 2 days.

DNA and glycosaminoglycan contents

Samples were digested in a papain solution at 60°C for 16 h. The DNA content was quantified using a fluorescence assay with Hoechst 33258 dye according to the manual (Sigma). The glycosaminoglycan (GAG) content was quantified using shark chondroitin sulfate standard following a published method.[18]

Scanning electron microscopy

The scaffolds and cell–scaffold constructs were rinsed in PBS, fixed with 2.5% glutaraldehyde and 2% paraformaldehyde overnight, postfixed with 1% osmium tetroxide, and dehydrated in increasing concentrations of ethanol and hexamethyldisilizane. The specimens were then sputter-coated with gold and observed under an SEM (Philips XL30 FEG) at an accelerating voltage of 10 kV.

Subcutaneous implantation

The animal procedures were approved by the University Committee on Use and Care of Animals (UCUCA) at the University of Michigan. Rabbit NP cell–scaffold constructs were cultured for 3 weeks *in vitro* before implantation. Randomized NF and SW scaffold–cell constructs (3.2 mm in diameter, 2 per mouse) were implanted subcutaneously on the dorsa of 6–8-week-old male nude mice (Charles River Laboratories, Wilmington, MA).[27] Four samples were implanted for each group. At 4 weeks, the mice were euthanized and the implants were harvested for analyses.

Rat caudal disc repair

Twenty four 3-month-old male athymic nude rats (Charles River Laboratories, Wilmington, MA) were divided into four groups: a normal control group, a sham control group (removing NP without implantation), an NF scaffold implant group, and an SW scaffold implant group. The surgery protocol was also approved by UCUCA.

The scaffolds were cut into an NP-like shape with a height of 1.0 mm and a diameter of 2.5 mm. Nine microliters cell suspension (3×10^7 NP cells/mL) was seeded on each scaffold. The constructs were cultured *in vitro* for 3 weeks before implantation.

Rats were anesthetized by inhaling isofluorane and medicated with buprenorphine (0.01 mg/kg body weight). A longitudinal incision (~3-cm long) was made to expose the native disc between the caudal segments 2 and 3 (Fig. 1A). The NP was removed, and the adjacent vertebral bodies were minimally retracted to allow the insertion of the NP implant into the disc space. The annulus was carefully closed with two 6.0 resorbable sutures (Fig. 1B). Finally, the tail skin was closed using resorbable sutures. Buprenorphine (0.01–0.02 mg/kg) was administered subcutaneously as needed. After 12 weeks, the rats were euthanized and the discs were harvested for analyses.

Radiographic analysis

Radiographs were taken at 2-week intervals up to 12 weeks after implantation. All radiographic images were analyzed

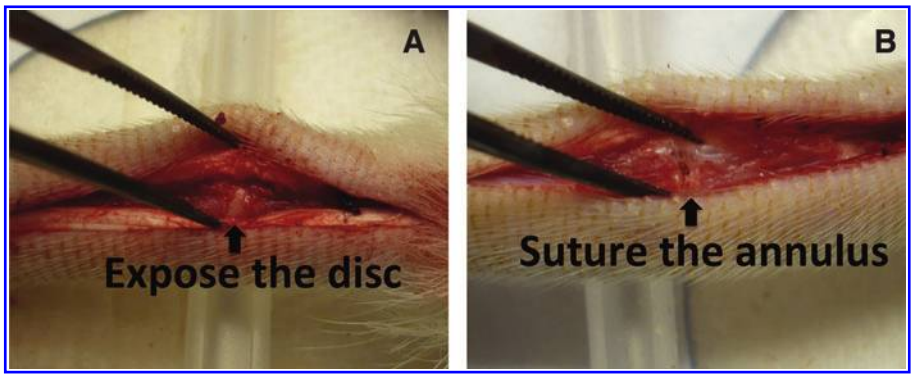

FIG. 1. Intraoperative images showing an exposed caudal disc **(A)** and the sutured annulus fibrosus **(B)**. After implanted with engineered nucleus pulposus (NP) (from either a nanofibrous [NF] scaffold or a solid-walled [SW] scaffold), the annulus is closed carefully with 6.0 resorbable sutures. In the sham control group, the NP was removed and the annulus was closed without any implant. Color images available online at www.liebertpub.com/tea

using ImageJ software (NIH, Bethesda, MD). The disc height index (DHI) was determined using a published method.[29] Changes in the DHI were expressed as %DHI and normalized to the measured preoperative DHI (%DHI = 100 × postoperative DHI/preoperative DHI).

Histological and immunohistochemical analyses

The specimens were fixed, decalcified (only for specimens from caudal disc repair model), dehydrated, and subsequently embedded in paraffin. Sections (5 μm thick) were stained using safranin-O and fast green for NP matrix and using Masson's trichrome method for collagen accumulation. Immunohistochemical analysis was carried out for type II and type I collagen.[30]

To quantify the histological results, we calculated the histological scores based on the method of Masuda *et al*.[31,32] Briefly, the slides were graded based on the histological appearance of four parameters: the annulus fibrosus, the border between the annulus fibrosus and the NP, the NP cellularity, and the NP matrix. Each of the four parameters was given a grade of 1, 2, or 3 (1 is the best and 3 is the worst). The sum of the grades for all parameters yielded a total score of 4 (the best) to 12 (the worst).

Statistical analysis

All data were presented as mean ± standard deviation. The Student's *t*-test was used to compare the differences between the study groups. A value of $p < 0.05$ was considered to be statistically significant.

Results

Preparation of NF-PLLA scaffolds and SW-PLLA scaffolds

Both the NF and SW scaffolds had similar interconnected macroporous structures and similar porosities of 96% (Fig. 2A, B). The only difference was in the wall architecture of macropores, being either NF or SW (Fig. 2C, D). The diameter of the nanofibers ranged from 50 to 500 nm, which is the same as that of natural collagen fibers.

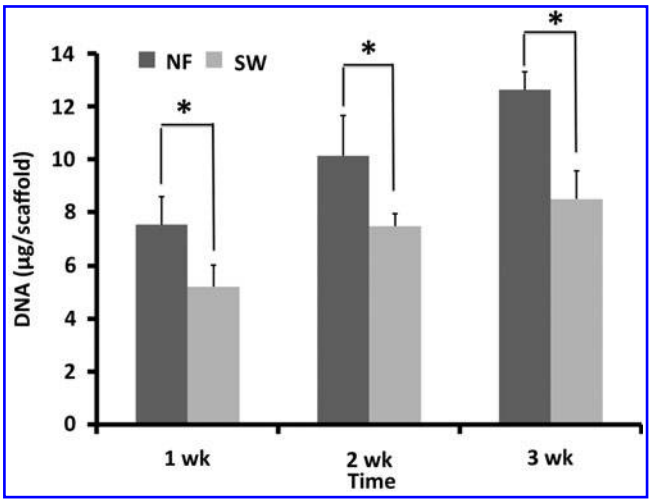

FIG. 3. The DNA content on NF scaffolds was significantly higher than that on SW scaffolds during the 3 weeks in culture (*$p < 0.05$).

Cellularity and ECM accumulation in vitro

The DNA measurement showed that there were more cells in the NF scaffolds than in the SW scaffolds during the 3 weeks in culture (Fig. 3). The ECM production on scaffolds was examined by safranin-O and immunohistochemical staining after in culture for 3 weeks. A stronger staining by safranin-O was found in the NF group (Fig. 4A–D), indicating more GAG deposition on NF scaffolds than that on SW scaffolds. Immunohistochemical staining revealed more

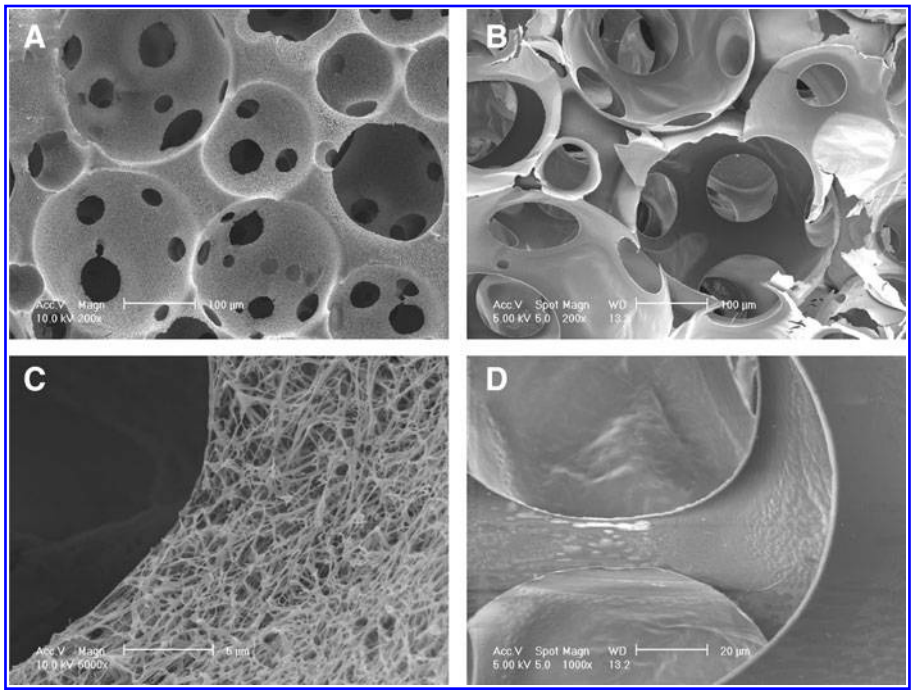

FIG. 2. SEM images of NF and SW scaffolds. **(A)** Macroporous structure of NF scaffolds at low magnification; **(B)** macroporous structure of SW scaffolds at low magnification; **(C)** NF architecture at high magnification; **(D)** SW architecture at high magnification.

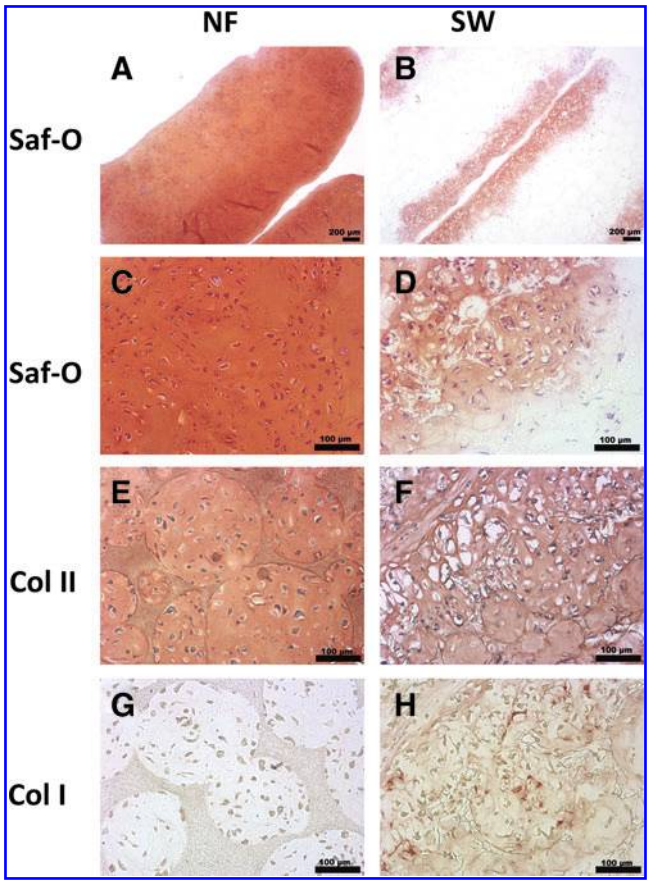

FIG. 4. Histological analysis of *in vitro* NP formation on NF and SW scaffolds. Constructs were cultured *in vitro* for 3 weeks. Cross sections were stained by safranin-O or immunohistochemical methods. Compared with SW scaffolds, NF scaffolds showed a stronger and more even staining by safranin-O method **(A, B)**. Higher magnification view showed increased cellular organization on the NF scaffolds when compared with SW scaffolds **(C, D)**. Immunohistochemical staining also revealed that the NF scaffold group was stained stronger for type II collagen **(E, F)**, but weaker for type I collagen than the SW scaffold group **(G, H)**. Color images available online at www.liebertpub.com/tea

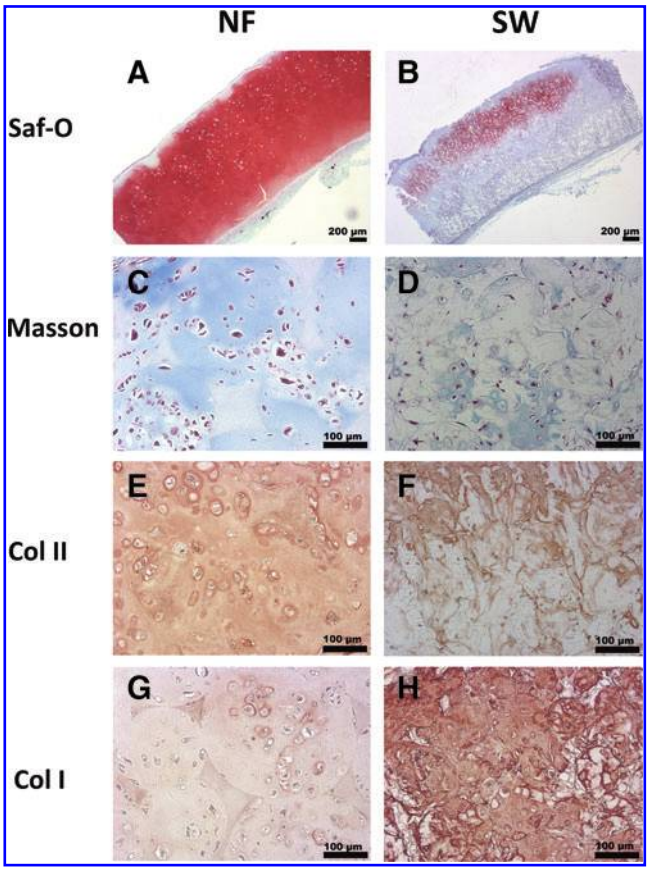

FIG. 5. Histological analysis of ectopic NP tissue formation *in vivo*. Four weeks after subcutaneous implantation of either the NF or the SW constructs, the tissue sections were stained with safranin-O for glycosaminoglycan (GAG) **(A, B)**, Masson's trichrome for total collagen **(C, D)**, and immunohistochemically stained for type I/II collagen **(E–H)**. Abundant GAG and type II collagen, while little type I collagen, were found in engineered tissue using the NF scaffold. In contrast, lower contents of GAG and type II collagen indicated poor NP formation from the SW scaffold group. At the same time, abundant deposition of type I collagen on the SW scaffold indicated fibrous tissue invasion in the SW scaffold group. Color images available online at www.liebertpub.com/tea

type II collagen, but less type I collagen in the NF group than in the SW group (Fig. 4 E–H).

Subcutaneous implantation

After each scaffold was seeded with the same number of NP cells, the cell–scaffold constructs were cultured *in vitro* for 3 weeks and then implanted subcutaneously in nude mice for 4 weeks. The safranin-O staining revealed more GAG deposition on the NF scaffolds than on the SW scaffolds (Fig. 5A, B). The total collagen synthesis in the two types of scaffolds was examined using Masson's trichrome staining. Blue-stained dense collagen matrix was observed inside the macropores of the NF scaffolds, while sparse collagen matrix was observed in SW scaffolds (Fig. 5C, D). Samples from the NF scaffolds were stained strongly for type II collagen and weakly for type I collagen (Fig. 5E, F). In contrast, samples from the SW scaffolds were stained strongly for type I collagen and weakly for type II collagen (Fig. 5G, H). Consistent with the histology result, significantly higher GAG contents were found in the NF group than in the SW group at both 2 and 4 weeks (Fig. 6).

Athymic rat caudal disc repair

The dissected spines in the normal control group showed a well-defined translucent central NP and a clearly defined annulus fibrousus (Fig. 7A). The disc in the sham control group failed rapidly, with complete collapse of the disc space resulting in interbody fusion (Fig. 7B). The NF scaffold implant group appeared similar to the normal control group in disc space maintenance and the matrix translucency (Fig. 7C). In the SW scaffold implant group, narrowing disc space and fibrous tissue invasion were observed (Fig. 7D). Consistently, the X-ray image indicated that the disc height in the NF scaffold group was similar to that in the normal control group. The SW scaffold group showed degenerative characteristics with narrowed disc height. In the sham control

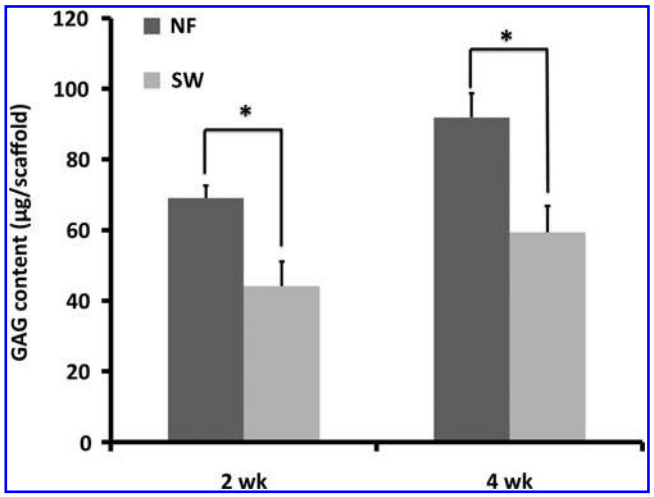

FIG. 6. GAG accumulation during ectopic NP formation. GAG content was quantified for constructs after subcutaneous implantation for 2 and 4 weeks. The GAG content increased with implantation time. Significantly more GAG was found on the NF constructs than on the SW constructs at the same time points ($*p < 0.05$).

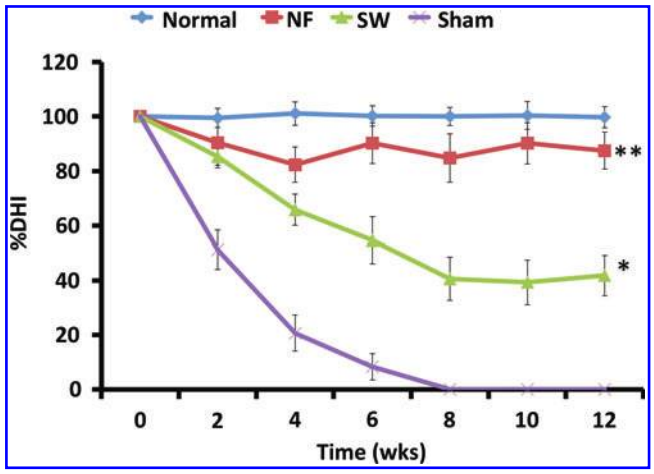

FIG. 8. The disc height index (DHI) changed with the time. The DHI in the NF scaffold group was comparable to that in the normal control group over the 12 weeks. $*p < 0.05$ between the NF scaffolds group and SW scaffolds group; $**p < 0.01$ between NF scaffolds group and sham control group. Color images available online at www.liebertpub.com/tea

group, the disc space almost disappeared completely and osteophytes formed at the margins of the vertebral bodies (Fig. 7E–H).

The DHI in the sham control group decreased dramatically during the first 2 weeks after operation, decreased at a slower rate after that, and was negligible (fused) at 8 weeks (Fig. 8). The DHI in the NF scaffold group was comparable to that in the normal control group over the 12 weeks. The DHI in the NF scaffold group was statistically higher than those in the sham control group and SW scaffold group at 4 weeks and thereafter. The DHI in the SW scaffold group was significantly higher than that in the sham control group after 2 weeks.

In the intact disc of normal control group, the boat-shaped NP occupied a large volume of the disc space and was stained strongly with safranin-O (Fig. 9A, E). The annulus fibrosus displayed a normal pattern of fibrocartilage lamellas and a well-defined border between the annulus fibrosus and the NP (Fig. 9I). Abundant ECM was deposited in the NP space in the NF scaffold group, which was similar to the intact disc (Fig. 9B, F). The cellularity in the engineered NP could be optimized by varying the amount of seeding cells. The histological appearance of annulus fibrosus in the NF group was also similar to that of the normal control group although with a slightly wavy structure (Fig. 9J). There was a much smaller residue of the NF scaffold than that of the SW scaffold, likely resulted from the faster degradation rate of NF scaffolds.[33] In the SW group, the NP area was hypocellular and consisted of larger areas of fibrous tissue, and was negative for safranin-O staining (Fig. 9C, G). A serpentine

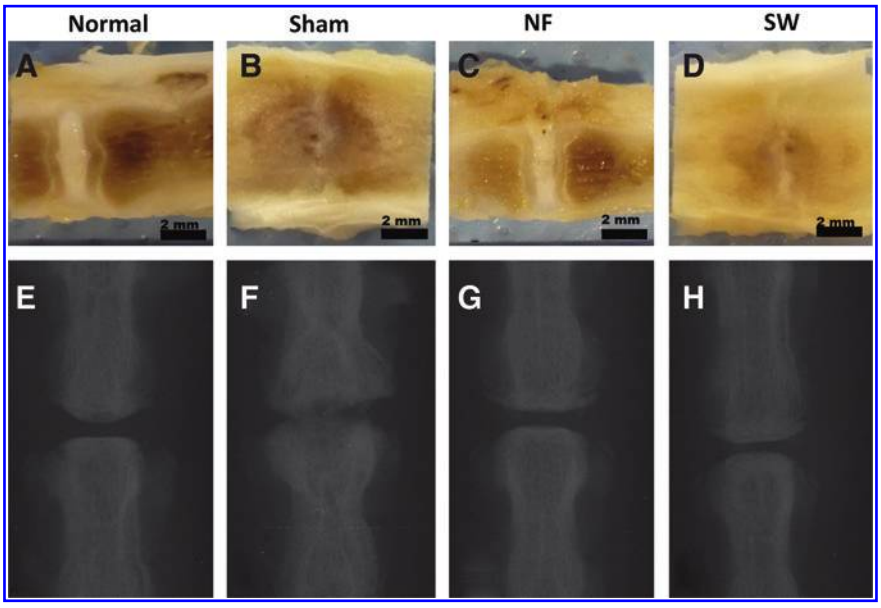

FIG. 7. Representative gross appearance and x-ray images of rat caudal spines at 12 weeks after operation: normal control **(A, E)**, sham control **(B, F)**, NF scaffold group **(C, G)**, and SW scaffold group **(D, H)**. A translucent matrix in the central area and a well-preserved disc height in the NF scaffold group indicated good NP regeneration. The x-ray results indicated that the disc height in the NF scaffold group was similar to that in the normal control group. The SW scaffold group showed disc degenerative characteristics with significantly narrowed disc height. In the sham control group, the disc space almost disappeared and an intervertebral fusion was observed. Color images available online at www.liebertpub.com/tea

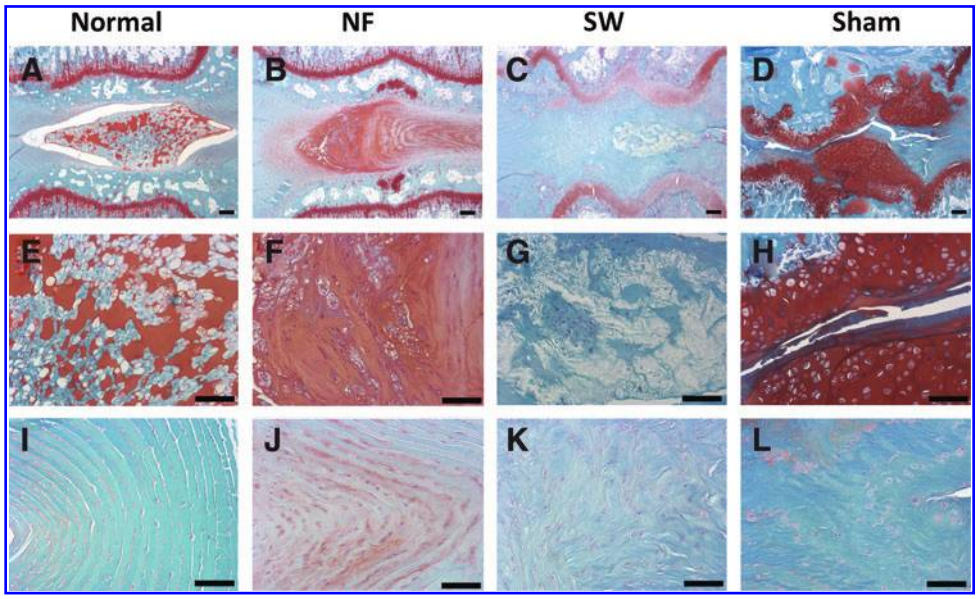

FIG. 9. Representative safranin-O/fast green stained samples from different experimental groups at 12 weeks after operation in rat caudal spines. In the normal disc **(A, E, I)**, the boat-shaped NP comprised a large area in the disc space and was stained strongly for safranin-O **(A, E)**. The annulus fibrosus displayed a normal pattern of fibrocartilage lamellas **(I)**. In the NF scaffold group **(B, F, J)**, the engineered NP contained abundant new extracellular matrix **(B, F)**, and the annulus was similar to the normal group although with a slightly wavy structure **(J)**. In the SW group **(C, G, K)**, the engineered NP was hypocellular and consisted of larger areas of fibrous tissue **(C, G)**, the annulus showed a serpentine appearance **(K)**. In the sham control group **(D, H, L)**, the nucleus pulpous structure nearly completely disappeared and the disc space was collapsed **(D)**, with evident inhomogeneous tissue invasion **(H)**. The annulus fibrosus in this group showed a severe serpentine appearance **(L)**. The scale bars represent 200 μm in **(A–D)**, 100 μm in **(E–L)**. Color images available online at www.liebertpub.com/tea

appearance of annulus fibrosus was noted in the SW group (Fig. 9K). In the sham control group, no repair tissue was detected. The disc space collapsed, with evident inhomogeneous tissue invasion and intervertebral fusion (Fig. 9D, H). A severe serpentine appearance of annulus fibrosus was found in the sham control group (Fig. 9L). The histological scores of the NF group were significantly lower than those in the sham control group or SW group, indicating a better regeneration outcome in the NF group (Fig. 10).

Discussion

The replacement of degenerated NP with engineered living NP would be highly desired.[27,34,35] The main challenges in developing a tissue-engineered NP implant are: (1) increasing NP cells and maintaining their phenotype; (2) providing a 3D template that guides the NP tissue formation; and (3) achieving the physiological function of the implants. Here we have demonstrated that our tissue-engineered NP implants are promising to meet these challenges.

In the normal NP, collagen fibers play an important role in the maintenance of normal disc structure and function. When the disc degenerates, the collagen breakdown results in loss of structural integrity, decrease in hydration, and subsequent further impairment of disc function.[36] To regenerate a biological NP replacement implant, a scaffold is required.[35] To provide a good environment for NP regeneration, we fabricated NF scaffolds to emulate the nanosized architecture of collagen fibers.

There is a serious shortage of NP cells, because a limited cell number can be harvested from an intervertebral disc and these cells proliferate slowly and lose their phenotypic characteristics in a monolayer culture.[37] In our study, a significantly higher number of cells was found in the NF scaffolds than in the control SW scaffolds during *in vitro* cultivation. Because the same number of cells was seeded on both the NF and the SW scaffolds, this result demonstrated that the NF scaffold enhanced the proliferation of NP cells. Therefore, in addition to advantageously supporting NP

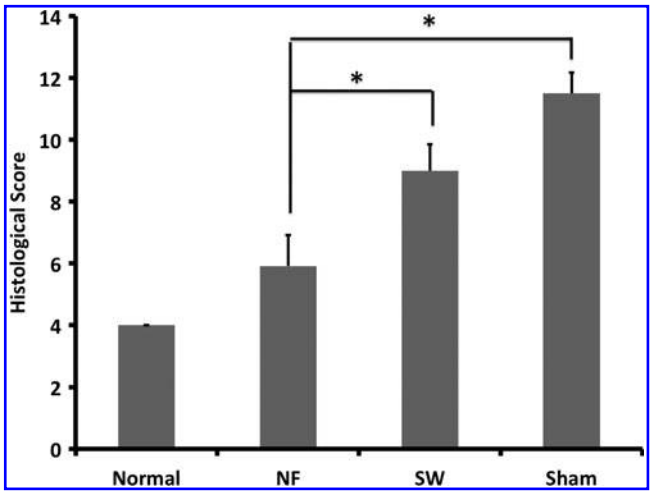

FIG. 10. The histological scores at 12 weeks after operation. Changes in histological appearance were assessed semi-quantitatively. Total grades ranged from 4 to 12, with 12 representing severe degeneration. *$p < 0.01$.

tissue regeneration, the NF scaffold could be utilized both to expand the cell population and to maintain the NP phenotype.

GAGs and type II collagen are the primary macromolecules that make up the ECM of the NP, which plays a key role in maintaining the normal physiological function of the intervertebral disc.[38,39] In our study, greater amounts of ECM production were associated with cells cultured on the NF scaffolds, indicating the advantages of the scaffolds that mimic the ECM architecture.

Various studies have examined ECM production associated with NP graft *in vitro*.[13–20,27,40–42] However, there has been no report on tissue-engineered NP replacement implants in the native disc space. The ability of the NP implants from the NF scaffolds to maintain the normal disc height is an important achievement, because preservation of disc height is a major clinical parameter to evaluate disc function. There are likely a number of contributing factors to the success of the NP replacement implant regenerated using NF scaffolds. Our previous studies demonstrated that NF scaffolds adsorbed greater amounts of cell adhesion proteins than SW scaffolds, which possibly activate intracellular signaling.[43] The NF architecture possibly also supported favorable cell morphology to maintain the differentiated NP phenotype.[30,44] Another possible contributing factor might be the local mass transport conditions. The high permeability, associated with channels between nanofibers, might allow for improved nutrient supply and metabolic waste removal. Further studies are needed to fully understand the underlying mechanisms of how the NF scaffold advantageously supports the NP tissue regeneration.

It is worth noting that despite the similarities in ECM content between the native and engineered NP, a number of differences exist. These include the imperfect NP structure, variation in NP volume, and the somewhat altered annulus fibrosus structure. Further improvements are needed.

In conclusion, the experimental data demonstrate that the NF architecture not only enhances NP cell function *in vitro*, but also facilitates NP tissue regeneration *in vivo*. The tissue-engineered NP can be implanted into the caudal spine, remains in place, produces functional ECM, and maintains the disc height, showing clinical potential.

Acknowledgments

The authors would like to acknowledge the financial support from the National Institutes of Health (Research Grants DE015384, DE017689, and DE022327: P.X.M.) and DOD (Research Grant W81XWH-12-2-0008: P.X.M.). This project was carried out entirely at the University of Michigan, and GF was a visiting graduate student partially supported by a fellowship from the China Scholarship Council.

Disclosure Statement

No competing financial interests exist.

References

1. Macfarlane, G.J., Thomas, E., Croft, P.R., Papageorgiou, A.C., Jayson, M.I., and Silman, A.J. Predictors of early improvement in low back pain amongst consulters to general practice: the influence of pre-morbid and episode-related factors. Pain **80,** 113, 1999.
2. Deyo, R.A., and Tsui-Wu, Y.J. Descriptive epidemiology of low-back pain and its related medical care in the United States. Spine **12,** 264, 1987.
3. Brisby, H. Pathology and possible mechanisms of nervous system response to disc degeneration. J Bone Joint Surg **88 Suppl 2,** 68, 2006.
4. Roberts, S., Evans, H., Trivedi, J., and Menage, J. Histology and pathology of the human intervertebral disc. J Bone Joint Surg **88 Suppl 2,** 10, 2006.
5. Hanley, E.N., Jr., and David, S.M. Lumbar arthrodesis for the treatment of back pain. J Bone Joint Surg **81,** 716, 1999.
6. Eismont, F.J., and Currier, B. Surgical management of lumbar intervertebral-disc disease. J Bone Joint Surg **71,** 1266, 1989.
7. Hilibrand, A.S., Carlson, G.D., Palumbo, M.A., Jones, P.K., and Bohlman, H.H. Radiculopathy and myelopathy at segments adjacent to the site of a previous anterior cervical arthrodesis. J Bone Joint Surg **81,** 519, 1999.
8. Park, P., Garton, H.J., Gala, V.C., Hoff, J.T., and McGillicuddy, J.E. Adjacent segment disease after lumbar or lumbosacral fusion: review of the literature. Spine **29,** 1938, 2004.
9. Lemaire, J.P., Skalli, W., Lavaste, F., Templier, A., Mendes, F., Diop, A., Sauty, V., and Laloux, E. Intervertebral disc prosthesis. Results and prospects for the year 2000. Clin Orthop Relat Res **337,** 64, 1997.
10. McAfee, P.C., Cunningham, B., Holsapple, G., Adams, K., Blumenthal, S., Guyer, R.D., Dmietriev, A., Maxwell, J.H., Regan, J.J., and Isaza, J. A prospective, randomized, multicenter Food and Drug Administration investigational device exemption study of lumbar total disc replacement with the CHARITE artificial disc versus lumbar fusion: part II: evaluation of radiographic outcomes and correlation of surgical technique accuracy with clinical outcomes. Spine **30,** 1576, 2005.
11. Di Martino, A., Vaccaro, A.R., Lee, J.Y., Denaro, V., and Lim, M.R. Nucleus pulposus replacement: basic science and indications for clinical use. Spine **30,** S16, 2005.
12. Klara, P.M., and Ray, C.D. Artificial nucleus replacement: clinical experience. Spine **27,** 1374, 2002.
13. Baer, A.E., Wang, J.Y., Kraus, V.B., and Setton, L.A. Collagen gene expression and mechanical properties of intervertebral disc cell-alginate cultures. J Orthop Res **19,** 2, 2001.
14. Chou, A.I., Akintoye, S.O., and Nicoll, S.B. Photo-cross-linked alginate hydrogels support enhanced matrix accumulation by nucleus pulposus cells *in vivo*. Osteoarthritis Cartilage **17,** 1377, 2009.
15. Chou, A.I., Bansal, A., Miller, G.J., and Nicoll, S.B. The effect of serial monolayer passaging on the collagen expression profile of outer and inner anulus fibrosus cells. Spine **31,** 1875, 2006.
16. Cloyd, J.M., Malhotra, N.R., Weng, L., Chen, W., Mauck, R.L., and Elliott, D.M. Material properties in unconfined compression of human nucleus pulposus, injectable hyaluronic acid-based hydrogels and tissue engineering scaffolds. Eur Spine J **16,** 1892, 2007.
17. Gruber, H.E., Ingram, J.A., Leslie, K., Norton, H.J., and Hanley, E.N., Jr. Cell shape and gene expression in human intervertebral disc cells: *in vitro* tissue engineering studies. Biotech Histochem **78,** 109, 2003.
18. Mizuno, H., Roy, A.K., Vacanti, C.A., Kojima, K., Ueda, M., and Bonassar, L.J. Tissue-engineered composites of anulus fibrosus and nucleus pulposus for intervertebral disc replacement. Spine **29,** 1290, 2004.

19. Reza, A.T., and Nicoll, S.B. Characterization of novel photocrosslinked carboxymethylcellulose hydrogels for encapsulation of nucleus pulposus cells. Acta Biomater **6,** 179, 2010.
20. Roughley, P., Hoemann, C., DesRosiers, E., Mwale, F., Antoniou, J., and Alini, M. The potential of chitosan-based gels containing intervertebral disc cells for nucleus pulposus supplementation. Biomaterials **27,** 388, 2006.
21. Pereira, D.R., Silva-Correia, J., Caridade, S.G., Oliveira, J.T., Sousa, R.A., Salgado, A.J., Oliveira, J.M., Mano, J.F., Sousa, N., and Reis, R.L. Development of gellan gum-based microparticles/hydrogel matrices for application in the intervertebral disc regeneration. Tissue Eng Part C Methods **17,** 961, 2011.
22. Sawamura, K., Ikeda, T., Nagae, M., Okamoto, S., Mikami, Y., Hase, H., Ikoma, K., Yamada, T., Sakamoto, H., Matsuda, K., Tabata, Y., Kawata, M., and Kubo, T. Characterization of *in vivo* effects of platelet-rich plasma and biodegradable gelatin hydrogel microspheres on degenerated intervertebral discs. Tissue Eng Part A **15,** 3719, 2009.
23. Richardson, S.M., Curran, J.M., Chen, R., Vaughan-Thomas, A., Hunt, J.A., Freemont, A.J., and Hoyland, J.A. The differentiation of bone marrow mesenchymal stem cells into chondrocyte-like cells on poly-L-lactic acid (PLLA) scaffolds. Biomaterials **27,** 4069, 2006.
24. Ma, P.X. Biomimetic materials for tissue engineering. Adv Drug Deliv Rev **60,** 184, 2008.
25. Gruber, H.E., Hoelscher, G., Ingram, J.A., and Hanley, E.N., Jr. Culture of human anulus fibrosus cells on polyamide nanofibers: extracellular matrix production. Spine **34,** 4, 2009.
26. Wei, G., and Ma, P.X. Macroporous and nanofibrous polymer scaffolds and polymer/bone-like apatite composite scaffolds generated by sugar spheres. J Biomed Mater Res Part A **78,** 306, 2006.
27. Feng, G., Jin, X., Hu, J., Ma, H., Gupte, M.J., Liu, H., and Ma, P.X. Effects of hypoxias and scaffold architecture on rabbit mesenchymal stem cell differentiation towards a nucleus pulposus-like phenotype. Biomaterial **32,** 8182, 2011.
28. Poiraudeau, S., Monteiro, I., Anract, P., Blanchard, O., Revel, M., and Corvol, M.T. Phenotypic characteristics of rabbit intervertebral disc cells. Comparison with cartilage cells from the same animals. Spine **24,** 837, 1999.
29. Lu, D.S., Shono, Y., Oda, I., Abumi, K., and Kaneda, K. Effects of chondroitinase ABC and chymopapain on spinal motion segment biomechanics. An *in vivo* biomechanical, radiologic, and histologic canine study. Spine **22,** 1828, 1997.
30. Liu, X., Jin, X., and Ma, P.X. Nanofibrous hollow microspheres self-assembled from star-shaped polymers as injectable cell carriers for knee repair. Nat Mater **10,** 398, 2011.
31. Masuda, K., Aota, Y., Muehleman, C., Imai, Y., Okuma, M., Thonar, E.J., Andersson, G.B., and An, H.S. A novel rabbit model of mild, reproducible disc degeneration by an anulus needle puncture: correlation between the degree of disc injury and radiological and histological appearances of disc degeneration. Spine **30,** 5, 2005.
32. Masuda, K., Oegema, T.R., Jr., and An, H.S. Growth factors and treatment of intervertebral disc degeneration. Spine **29,** 2757, 2004.
33. Chen, V.J., and Ma, P.X. The effect of surface area on the degradation rate of nano-fibrous poly(L-lactic acid) foams. Biomaterials **27,** 3708, 2006.
34. Nerurkar, N.L., Elliott, D.M., and Mauck, R.L. Mechanical design criteria for intervertebral disc tissue engineering. J Biomech **43,** 1017, 2010.
35. O'Halloran, D.M., and Pandit, A.S. Tissue-engineering approach to regenerating the intervertebral disc. Tissue Eng **13,** 1927, 2007.
36. Crean, J.K., Roberts, S., Jaffray, D.C., Eisenstein, S.M., and Duance, V.C. Matrix metalloproteinases in the human intervertebral disc: role in disc degeneration and scoliosis. Spine **22,** 2877, 1997.
37. Horner, H.A., Roberts, S., Bielby, R.C., Menage, J., Evans, H., and Urban, J.P. Cells from different regions of the intervertebral disc: effect of culture system on matrix expression and cell phenotype. Spine **27,** 1018, 2002.
38. Miyazaki, T., Kobayashi, S., Takeno, K., Meir, A., Urban, J., and Baba, H. A phenotypic comparison of proteoglycan production of intervertebral disc cells isolated from rats, rabbits, and bovine tails; which animal model is most suitable to study tissue engineering and biological repair of human disc disorders? Tissue Eng Part A **15,** 3835, 2009.
39. Nesti, L.J., Li, W.J., Shanti, R.M., Jiang, Y.J., Jackson, W., Freedman, B.A., Kuklo, T.R., Giuliani, J.R., and Tuan, R.S. Intervertebral disc tissue engineering using a novel hyaluronic acid-nanofibrous scaffold (HANFS) amalgam. Tissue Eng Part A **14,** 1527, 2008.
40. Cheng, Y.H., Yang, S.H., Su, W.Y., Chen, Y.C., Yang, K.C., Cheng, W.T., Wu, S.C., and Lin, F.H. Thermosensitive chitosan-gelatin-glycerol phosphate hydrogels as a cell carrier for nucleus pulposus regeneration: an *in vitro* study. Tissue Eng Part A **16,** 695, 2010.
41. Gaetani, P., Torre, M.L., Klinger, M., Faustini, M., Crovato, F., Bucco, M., Marazzi, M., Chlapanidas, T., Levi, D., Tancioni, F., Vigo, D., and Rodriguez y Baena, R. Adipose-derived stem cell therapy for intervertebral disc regeneration: an *in vitro* reconstructed tissue in alginate capsules. Tissue Eng Part A **14,** 1415, 2008.
42. Gupta, M.S., Cooper, E.S., and Nicoll, S.B. Transforming growth factor-beta 3 stimulates cartilage matrix elaboration by human marrow-derived stromal cells encapsulated in photocrosslinked carboxymethylcellulose hydrogels: potential for nucleus pulposus replacement. Tissue Eng Part A **17,** 2903, 2011.
43. Woo, K.M., Chen, V.J., and Ma, P.X. Nano-fibrous scaffolding architecture selectively enhances protein adsorption contributing to cell attachment. J Biomed Mater Res Part A **67,** 531, 2003.
44. Hu, J., Feng, K., Liu, X., and Ma, P.X. Chondrogenic and osteogenic differentiations of human bone marrow-derived mesenchymal stem cells on a nanofibrous scaffold with designed pore network. Biomaterials **30,** 5061, 2009.

Address correspondence to:
Peter X. Ma, Ph.D.
Department of Biologic and Materials Sciences
The University of Michigan
1011 North University Ave., Room 2211
Ann Arbor, MI 48109-1078

E-mail: mapx@umich.edu

Received: December 30, 2011
Accepted: May 30, 2012
Online Publication Date: August 8, 2012

This article has been cited by:

1. G. Feng, L. Li, H. Liu, Y. Song, F. Huang, C. Tu, B. Shen, Q. Gong, T. Li, L. Liu, J. Zeng, Q. Kong, M. Yi, M. Gupte, P.X. Ma, F. Pei. 2013. Hypoxia differentially regulates human nucleus pulposus and annulus fibrosus cell extracellular matrix production in 3D scaffolds. *Osteoarthritis and Cartilage* **21**:4, 582-588. [CrossRef]